

Geometric description of the Kitaev honeycomb lattice model

Ashk Farjami,^{1,†} Matthew D. Horner,^{1,†} Chris N. Self,^{1,2} Zlatko Papić,¹ and Jiannis K. Pachos¹

¹*School of Physics and Astronomy, University of Leeds, Leeds, LS2 9JT, United Kingdom*

²*Blackett Laboratory, Imperial College London, Prince Consort Road, London, SW7 2AZ, United Kingdom*

(Dated: October 20, 2022)

It is widely accepted that topological superconductors can only have an effective interpretation in terms of curved geometry rather than gauge fields due to their charge neutrality. This approach is commonly employed in order to investigate their properties, such as the behaviour of their energy currents. Nevertheless, it is not known how accurately curved geometry can describe actual microscopic models. Here, we demonstrate that the low-energy properties of the Kitaev honeycomb lattice model – a topological superconductor that supports localised Majorana zero modes at its vortex excitations – are faithfully described in terms of Riemann-Cartan geometry. In particular, we show analytically that the continuum limit of the model is given in terms of the Majorana version of the Dirac Hamiltonian coupled to both curvature and torsion. We numerically establish the accuracy of the geometric description for a wide variety of couplings of the microscopic model. Our work opens up the opportunity to accurately predict dynamical properties of the Kitaev model from its effective geometric description.

I. INTRODUCTION

In recent years there has been a surge of interest in the geometrical degrees of freedom that characterise the response of topologically-ordered phases of matter beyond the well-known limit governed by an effective topological quantum field theory. An important class of such systems, the fractional quantum Hall (FQH) states, have been understood to exhibit a universal response to the variations of ambient geometry, leading to many fruitful investigations of an interplay between topology and geometry in these strongly-correlated systems^{1–11}. In particular, the neutral collective mode of FQH systems¹² has been described as a fluctuating spacetime metric^{13–15}. On the other hand, a recent study¹⁶ has shown that by minimally coupling a spinless p -wave superconductor on a square lattice to an electromagnetic field, the continuum limit takes the form of a Dirac Hamiltonian defined on a spacetime with both curvature and torsion. Such curved spaces with torsion are called *Riemann-Cartan* spacetimes¹⁷. Riemann-Cartan geometry also naturally arises in the theory of defects in lattices, whereby disclinations and dislocations in the continuum limit are described by curvature and torsion, respectively^{18,19}. Other techniques from quantum gravity have also been employed in condensed matter such as the holographic correspondence or AdS/CFT correspondence. Recently, the holographic correspondence has been used to model gapless modes living on the defect lines of class D topological superconductors²⁰ and to determine the specific heat of a two-dimensional interacting gapless Majorana system²¹. Moreover, the emergence of gravitational anomalies has been considered in topological superconductors²². Building upon Luttinger’s proposal²³, gravitational techniques applied to the thermal Hall effect have also attracted many theoretical^{24–30} and experimental^{31,32} investigations.

Nevertheless, despite much progress in the investigation of geometric effects in the continuum field theory

description, the study of Riemann-Cartan geometry in microscopic, solvable lattice models has received less attention. In this paper, we investigate geometric description of the Kitaev honeycomb lattice model (KHLM)³³, the well-known two-dimensional (2D) model of interacting spin- $\frac{1}{2}$ particles that gives rise to a quantum spin liquid phase with topological order. A salient feature of the KHLM is that it can support non-Abelian anyons in the form of Majorana zero modes (MZMs) trapped at its vortices^{33–35}. Similar to the FQH effect³⁶, the KHLM is both topologically ordered in the sense that it can support anyonic excitations and it is a topological phase with a non-trivial Chern number³³. Unlike the FQH effect, the KHLM is exactly solvable, which has provided unique opportunities to analytically probe its anyonic properties³⁷, its topological edge currents³⁸, and to investigate its finite temperature behaviour^{39–44}. Moreover, many features of the KHLM are recognised in experimentally realisable materials, such as complex iridium oxides^{45–47} or ruthenium chloride⁴⁸. This makes the KHLM of interest to numerous theoretical and experimental investigations.

In this paper we address the following question: can we use the KHLM to simulate Majorana fermions embedded in a Riemann-Cartan spacetime? To answer this question, we allow the couplings of the KHLM to take general configurations that are anisotropic and inhomogeneous, while leaving the lattice configuration of the model unaffected. We demonstrate that in this case the low energy limit of the model can be effectively described by massless Majorana spinors obeying the Dirac equation embedded in a Riemann-Cartan spacetime which is locally Lorentz invariant. Moreover, the Majorana spinors are coupled to a non-trivial torsion. It is important to stress that this geometry emerges purely from distortions in the couplings of the system and *not* from the geometry of the lattice itself.

We shall see that choosing the two-spin couplings to be anisotropic gives rise to a general two-dimensional metric. When these couplings are varying in space they

can give rise to an arbitrary curved space. Moreover, the three-spin interactions generate the torsion of the Riemann-Cartan geometry. As a result, the KHLM can be effectively described by massless relativistic Majorana spinors. These particles become massive when a Kekulé distortion is introduced in the two-spin couplings⁴⁹. We numerically investigate the phase diagram produced by the torsion and mass terms that support competing topological phases.

To quantify how faithful the geometric description is to the KHLM we consider two physical quantities of the original microscopic model. First, we investigate the spatial distribution of the quantum correlations in the ground state of the model. Second, we analyse the shape of a Majorana zero mode bounded by a vortex. While we vary the couplings of the model away from the isotropic regime we numerically observe that the geometric distortion of the quantum correlations as well as shape of the zero mode follow the theoretically predicted geometric configurations. This agreement is faithful through most of the non-Abelian phase only breaking down near the phase transition boundaries. Hence, the Riemann-Cartan description can be employed to accurately describe the behaviour of the KHLM in a quantum field theory language. This opens up the exciting possibility to theoretically study response properties of KHLM, such as the energy currents as a function of coupling distortions or temperature gradients, in a quantitative way.

The paper is organised as follows. In Section II we provide a self-contained introduction to the KHLM and demonstrate that the low energy limit of the model is described by massless Majorana fermions satisfying the Dirac Hamiltonian. In Section III we review the relevant theory of Majorana spinors defined on a Riemann-Cartan geometry and derive the corresponding Hamiltonian. In Section IV we demonstrate that the low energy limit of the KHLM can be faithfully described by massless Majorana fermions propagating on a Riemann-Cartan background, with geometric characteristics fully determined by the coupling constants of the model. We also present the Kekulé distortion modification to the KHLM, which is responsible for generating mass in the continuum limit. In Section V we present numerical results of correlation functions and zero mode profiles for various coupling configurations of the KHLM in order to verify its non-trivial description in terms of a metric. Finally in Section VI we present the conclusions and an outlook of our work.

II. KITAEV HONEYCOMB LATTICE MODEL IN THE CONTINUUM

Similar to graphene^{50–52}, the KHLM with isotropic, homogeneous couplings has a continuum limit that is given in terms of a Dirac Hamiltonian. To reveal this feature we consider the low energy sector of the model where long wavelengths are dominant and the lattice spacing is negligible. In this low energy regime the KHLM can be

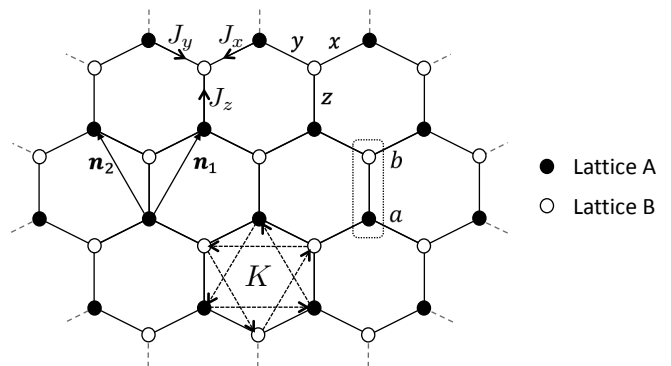


FIG. 1. The honeycomb lattice with Majorana fermions tunnelling between nearest neighbouring sites with couplings J_x , J_y and J_z depending on the direction of the link. Tunnelling between next-to-nearest neighbouring sites with coupling K is also indicated. The honeycomb lattice comprises two triangular sub-lattices, A and B, denoted by full and empty circles, respectively. We take the unit cell along the z -links. The translation vectors between sites of the same sub-lattices are $\mathbf{n}_1 = (\frac{\sqrt{3}}{2}, \frac{3}{2})$ and $\mathbf{n}_2 = (-\frac{\sqrt{3}}{2}, \frac{3}{2})$. The orientations of the nearest tunnelings (from A to B sites) and next-to-nearest tunnelings (anticlockwise) are indicated.

efficiently described by a linear energy dispersion relation. This linearity between energy and momentum can be modelled by the Dirac Hamiltonian. For the case of the KHLM, this Dirac Hamiltonian can take a purely imaginary form signalling that the effective degrees of freedom of the model are Majorana fermions. As a result, the model is faithfully described by a quantum field theory of relativistic Majorana fermions. We will review this derivation here in order to set our notation for the later sections.

Kitaev's honeycomb lattice is an exactly solvable model that describes interacting spin- $\frac{1}{2}$ particles residing on the vertices of a honeycomb lattice³³. The spin couplings consist of nearest and next-to-nearest neighbour interactions described by the Hamiltonian

$$H = -4 \left(J_x \sum_{x \text{ links}} \sigma_i^x \sigma_j^x + J_y \sum_{y \text{ links}} \sigma_i^y \sigma_j^y + J_z \sum_{z \text{ links}} \sigma_i^z \sigma_j^z + K \sum_{(i,j,k)} \sigma_i^x \sigma_j^y \sigma_k^z \right), \quad (1)$$

where the orientation of the x -links, y -links and z -links are indicated in Fig. 1. In Eq. (1) we have introduced a factor of 4 compared to Ref. 33 in order to simplify the subsequent algebra. The three spin interaction acts between three successive spins around a hexagonal plaquette³³. For certain values of the couplings $\{J_i\}$ and K , the ground state of the model is a quantum spin liquid^{53–55}. This state exhibits exotic quantum order due to long-range entanglement, which leads to spin-fractionalised excitations that behave as Abelian or non-Abelian anyons³³.

By employing an appropriate fermionisation procedure, the spin Hamiltonian can be brought to a form describing Majorana fermions coupled to a \mathbb{Z}_2 gauge field. This gauge field can encode vortices which are eigenstates of the original spin Hamiltonian. Here, we shall restrict ourselves to the *no-vortex sector*, where the gauge field has a trivial configuration. In this case, the Hamiltonian takes the form

$$H = i \left(\sum_{\langle i,j \rangle} 2J_{ij} c_i c_j + 2K \sum_{\langle\langle i,j \rangle\rangle} c_i c_j \right), \quad (2)$$

where $\{c_i\}$ are Majorana fermions sitting on the site i . The first term of the Hamiltonian is a sum over nearest neighbours whilst the second term is a sum over next-to-nearest neighbours. The ordering of the Majorana operators for the nearest and next-to-nearest couplings is as shown in Fig. 1.

The honeycomb lattice contains two triangular sublattices, A and B , denoted in Fig. 1 by full and empty circles, respectively. With this identification, we denote the Majoranas of sub-lattice A as c_i^a and those of sub-lattice B as c_i^b , where now the index i labels a unit cell of two neighbouring sites along the z -direction, as shown in Fig. 1. The honeycomb lattice model is periodic with respect to this unit cell. We are able to diagonalise the Hamiltonian in Majorana form by taking its Fourier transform, through the definitions $c_{\mathbf{q}}^{a/b} = \int d^2q e^{-i\mathbf{q}\cdot\mathbf{r}_i} c_i^{a/b}$, where \mathbf{r}_i is the position of the cell i . If we define the two-component spinor $\psi_{\mathbf{q}} = (c_{\mathbf{q}}^a \ i c_{\mathbf{q}}^b)^T$, then the Hamiltonian takes the form $H = \int d^2q \psi_{\mathbf{q}}^\dagger h(\mathbf{q}) \psi_{\mathbf{q}}$, with the single-particle Hamiltonian $h(\mathbf{q})$ given by

$$h(\mathbf{q}) = \begin{pmatrix} \Delta(\mathbf{q}) & -f(\mathbf{q}) \\ -f^*(\mathbf{q}) & -\Delta(\mathbf{q}) \end{pmatrix}, \quad (3)$$

where

$$f(\mathbf{q}) = 2(J_x e^{i\mathbf{q}\cdot\mathbf{n}_1} + J_y e^{i\mathbf{q}\cdot\mathbf{n}_2} + J_z), \quad (4)$$

and

$$\Delta(\mathbf{q}) = 2K[-\sin(\mathbf{q}\cdot\mathbf{n}_1) + \sin(\mathbf{q}\cdot\mathbf{n}_2) + \sin(\mathbf{q}\cdot(\mathbf{n}_1 - \mathbf{n}_2))]. \quad (5)$$

For simplicity we initially consider the isotropic case where $J_x = J_y = J_z = J$. The dispersion relation of the single-particle Hamiltonian is given by

$$E(\mathbf{q}) = \pm \sqrt{\Delta^2(\mathbf{q}) + |f(\mathbf{q})|^2}. \quad (6)$$

For $K = 0$ the spectrum of $h(\mathbf{q})$ is plotted in Fig. 2. We see that the system has two independent Fermi points in the Brillouin zone located at

$$\mathbf{P}_{\pm} = \pm \left(\frac{4\pi}{3\sqrt{3}}, 0 \right). \quad (7)$$

When $K \neq 0$ this opens a gap in the dispersion $\Delta(\mathbf{P}_{\pm}) = \pm\Delta$, where $\Delta = -3\sqrt{3}K$. The presence of Fermi points

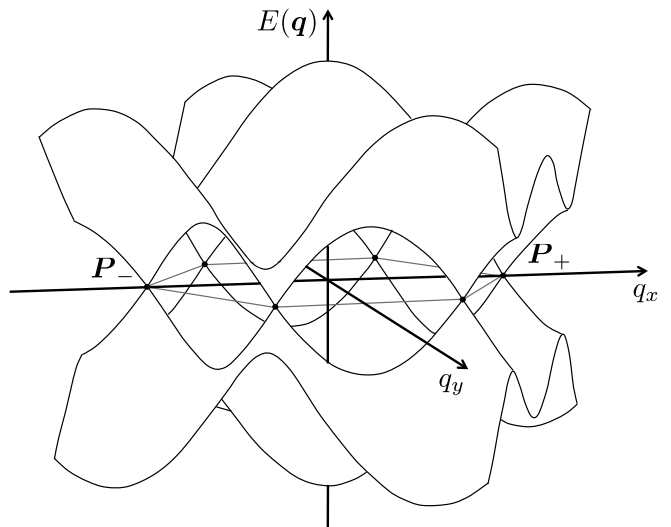


FIG. 2. The dispersion relation $E(\mathbf{q})$ for the honeycomb Hamiltonian when $J_x = J_y = J_z = J$ and $K = 0$. The Fermi points are the points where $E(\mathbf{q}) = 0$. The two inequivalent Fermi points within the Brillouin zone are given by \mathbf{P}_+ and \mathbf{P}_- .

enables us to analyse the low energy properties of the Kitaev model and extract its behaviour in the continuum limit.

In the regions close to the two Fermi points the Majorana fields have a linear dispersion relation much like the spectrum of graphene, as shown in Fig. 2. Hence, at low enough energies the Hamiltonian $h(\mathbf{q})$ can be effectively described by a Dirac Hamiltonian. In order to obtain this description, we substitute $\mathbf{q} = \mathbf{P}_{\pm} + \mathbf{p}$ for small \mathbf{p} and Taylor expand $h(\mathbf{q})$ around the Fermi points up to first order in \mathbf{p} . For convenience we define the Hamiltonian $h_{\pm}(\mathbf{p}) \equiv h(\mathbf{P}_{\pm} + \mathbf{p})$ for each Fermi point. For non-zero K we obtain

$$h_{\pm}(\mathbf{p}) = 3J(\pm\sigma^x p_x - \sigma^y p_y) \mp 3\sqrt{3}K\sigma^z + O(p^2), \quad (8)$$

which act on the spinors $\psi_+(\mathbf{p}) = (c_+^a \ i c_+^b)^T$ and $\psi_-(\mathbf{p}) = (c_-^a \ i c_-^b)^T$, respectively, where $c_{\pm}^{a/b} = c_{\mathbf{P}_{\pm}}^{a/b}$. As these two Hamiltonians need to be considered simultaneously, we can treat the two Fermi points as different chiral degrees of freedom by defining the Dirac-like spinor $\Psi(\mathbf{p}) = (c_+^a \ i c_+^b \ i c_-^b \ c_-^a)^T$. We take the direct sum of $h_+(\mathbf{p})$ and $h_-(\mathbf{p})$ in their respective bases defined by Ψ to yield the total 4×4 Hamiltonian

$$h_{\text{KHLM}}(\mathbf{p}) = 3J(\sigma^z \otimes \sigma^x p_x - \sigma^z \otimes \sigma^y p_y) - 3\sqrt{3}K\mathbb{I} \otimes \sigma^z. \quad (9)$$

Note that we have rotated $h_-(\mathbf{p})$ with a σ^x rotation before combining it with $h_+(\mathbf{p})$ to obtain $h_{\text{KHLM}}(\mathbf{p})$.

The low energy limit given by (9) suggests that we use the Dirac α and β matrices

$$\alpha = \begin{pmatrix} \sigma & 0 \\ 0 & -\sigma \end{pmatrix} = \sigma^z \otimes \sigma, \quad \beta = \begin{pmatrix} 0 & \mathbb{I} \\ \mathbb{I} & 0 \end{pmatrix} = \sigma^x \otimes \mathbb{I}, \quad (10)$$

where $\boldsymbol{\sigma} = (\sigma^x, \sigma^y, \sigma^z)$ are the Pauli matrices and \mathbb{I} is the two-dimensional identity. The corresponding Dirac gamma matrices are defined by $\gamma^0 = \beta$ and $\boldsymbol{\gamma} = \beta^{-1}\boldsymbol{\alpha}$ where

$$\boldsymbol{\gamma} = \begin{pmatrix} 0 & -\boldsymbol{\sigma} \\ \boldsymbol{\sigma} & 0 \end{pmatrix} = -i\boldsymbol{\sigma}^y \otimes \boldsymbol{\sigma}. \quad (11)$$

These matrices satisfy the Clifford algebra $\{\gamma^a, \gamma^b\} = 2\eta^{ab}$, where Latin indices $a, b, \dots \in (0, 1, 2)$ and $\eta_{ab} = \text{diag}(1, -1, -1)$ is the Minkowski metric.

Using the gamma matrices, the Hamiltonian (9) becomes

$$h_{\text{KHLM}}(\mathbf{p}) = 3J(\gamma^0\gamma^1p_x - \gamma^0\gamma^2p_y) - i3\sqrt{3}K\gamma^1\gamma^2. \quad (12)$$

By its turn the many-body Hamiltonian of the low energy limit is given by

$$H_{\text{KHLM}} = \int d^2p \Psi_{\mathbf{p}}^\dagger h_{\text{KHLM}}(\mathbf{p}) \Psi_{\mathbf{p}}, \quad (13)$$

where $\Psi_{\mathbf{p}}$ is a four-dimensional spinor. Hence, the low energy limit of the Kitaev model is given by the Dirac Hamiltonian with linear energy dispersion relation and an additional K -term that gives rise to an energy gap at the Fermi points.

To verify that the spinors of the Dirac operator are Majorana we first define charge conjugation. The charge conjugate of a Dirac spinor Ψ is defined as $\Psi^{(c)} = C\Psi^*$, where C is the charge conjugation matrix defined as a matrix satisfying $C^\dagger C = \mathbf{I}$ and $C\gamma^\mu C = -(\gamma^\mu)^*$ for all gamma matrices. In our chiral basis, the charge conjugation matrix is given by $C = -\sigma^y \otimes \sigma^y$. With this, we see that the spinor Ψ satisfies the neutrality condition $\Psi^{(c)} = \Psi$ and is therefore a Majorana spinor.

III. MAJORANA FIELD IN (2 + 1)-DIMENSIONAL RIEMANN-CARTAN GEOMETRY

As we have seen in the previous section, the KHLM describes Majorana fields in a flat Minkowski spacetime. We now consider a Majorana field in a *curved* spacetime. To proceed we first introduce the tools that allow us to transform from a flat space, where the usual Dirac Hamiltonian is defined, to a curved space. This can be achieved in three dimensions with the help of dreibein. We are in particular interested in a curved spacetimes that supports torsion, i.e. deformations of spacetime that cannot be described by a metric. These generalised spacetimes are called Riemann-Cartan. The following section closely follows references 56 and 57.

A. Riemann-Cartan Spacetime

1. Dreibein

Consider a $(2 + 1)$ -dimensional spacetime M with coordinate system (t, x, y) . At every point on M we have the coordinate basis vectors $\{e_\mu = \partial_\mu\}$ of the tangent spaces, together with their corresponding dual basis vectors $\{e^\mu = dx^\mu\}$ satisfying $e^\mu(e_\nu) = \delta_\nu^\mu$. We use *Greek* indices ranging over t, x, y to represent components of tensors with respect to the coordinate basis. When discussing spinors on a general spacetime we need the notion of an *orthonormal* basis. Given a metric tensor g , the dreibein basis is given by $\{e_a = e_a^\mu e_\mu\}$ with corresponding dual basis $\{e^a = e^a_\mu e^\mu\}$, which satisfies $g(e_a, e_b) = \eta_{ab}$ and $e^a(e_b) = \delta_b^a$, where $\eta_{ab} = \text{diag}(1, -1, -1)$ is the Minkowski metric. In components, these relations read

$$g_{\mu\nu}e_a^\mu e_b^\nu = \eta_{ab}, \quad e^a_\mu e_b^\mu = \delta_b^a. \quad (14)$$

We use *Latin* indices ranging over $0, 1, 2$ to represent components of tensors with respect to the dreibein basis.

The components of the dreibein e_a^μ themselves are sometimes called the dreibein, while the components of the dual dreibein e^a_μ are called the *inverse dreibein* as they allow one to invert the expressions (14). However, we adopt the convention of simply calling them both the dreibein. The dreibein also allow us to transform components between frames, i.e. for a $(1, 0)$ tensor A we have $A^\mu = e_a^\mu A^a$ and $A^a = e^a_\mu A^\mu$ and so on for higher rank tensors. The metrics $g_{\mu\nu}$ and η_{ab} and their inverses $g^{\mu\nu}$ and η^{ab} allow us to raise and lower Greek and Latin indices, respectively.

2. Spin Connection

The covariant derivative of a tensor is usually expressed in terms of the coordinate basis. For example, the covariant derivative of a rank $(1, 1)$ tensor A^μ_ν is given by

$$\nabla_\alpha A^\mu_\nu = \partial_\alpha A^\mu_\nu + \Gamma^\mu_{\beta\alpha} A^\beta_\nu - \Gamma^\beta_{\nu\alpha} A^\mu_\beta, \quad (15)$$

where $\Gamma^\alpha_{\beta\gamma}$ are the components of the *connection*. From this, we can extend the definition to tensors of arbitrary rank with a factor of $\Gamma^\alpha_{\beta\gamma}$ for each index of the tensor.

The choice of our connection defines what our covariant derivative is. It is commonplace to restrict to a *metric compatible* connection, that is, a connection for which $\nabla g = 0$. It can be shown that a metric compatible connection takes the form

$$\Gamma^\rho_{\mu\nu} = \tilde{\Gamma}^\rho_{\mu\nu} + K^\rho_{\mu\nu}, \quad (16)$$

where $\tilde{\Gamma}^\rho_{\mu\nu}$ is the *Levi-Civita* connection, sometimes called the *Christoffel symbols*, and $K^\rho_{\mu\nu}$ is the contortion tensor. The Levi-Civita connection is completely

determined by the metric

$$\tilde{\Gamma}^\rho_{\mu\nu} = \frac{1}{2}g^{\rho\sigma}(\partial_\mu g_{\sigma\nu} + \partial_\nu g_{\sigma\mu} - \partial_\sigma g_{\mu\nu}), \quad (17)$$

and is symmetric on exchange of μ and ν . On the other hand, the contortion tensor is given by

$$K^\rho_{\mu\nu} = \frac{1}{2}(T^\rho_{\mu\nu} + T^\rho_{\nu\mu} + T^\rho_{\mu\nu}). \quad (18)$$

where $T^\rho_{\mu\nu} = 2\Gamma^\rho_{[\mu\nu]}$ is the torsion tensor corresponding to the connection $\Gamma^\rho_{\mu\nu}$ and square brackets denote anti-symmetrisation over the indices contained within the bracket.

The tools introduced so far can be expressed in terms of the dreibein basis. The components of the *spin connection* are given by

$$\omega^a_{\mu b} = e^a_\alpha(\partial_\mu e_b^\alpha + \Gamma^\alpha_{\beta\mu} e_b^\beta). \quad (19)$$

In this case, analogous to (15), the covariant derivative of a (1,1) tensor A^a_b in the dreibein basis will be

$$\nabla_\mu A^a_b = \partial_\mu A^a_b + \omega^a_{\mu c} A^c_b - \omega^c_{\mu b} A^a_c. \quad (20)$$

The spin connection is also of interest to us as it allows one to take covariant derivatives of spinors which will be discussed in more detail in the next section.

If we work with a metric compatible connection given by (16), we see that the spin connection will expand out as

$$\omega^a_{\mu b} = \tilde{\omega}^a_{\mu b} + K^a_{\mu b}, \quad (21)$$

where $\tilde{\omega}^a_{\mu b}$ is the Levi-Civita spin connection related to the coordinate Levi-Civita connection via the formula (19) with $\Gamma^\alpha_{\beta\mu}$ replaced with $\tilde{\Gamma}^\alpha_{\beta\mu}$. The contortion tensor is just expressed in the dreibein basis as $K^a_{\mu b} = e^a_\rho e_b^\nu K^\rho_{\mu\nu}$. It can be shown that for a metric compatible connection, if we treat the dreibein e_a^μ as the components of a (1,1) tensor, then $\nabla_\mu e_a^\nu = 0$, which is known as the *dreibein postulate*.

3. Curvature and Torsion

The connection of a space also defines two extra geometric quantities, the curvature and the torsion. The torsion of a connection has already been defined as

$$T^\rho_{\mu\nu} = 2\Gamma^\rho_{[\mu\nu]}, \quad (22)$$

with respect to the coordinate basis. As the Levi-Civita connection $\tilde{\Gamma}^\rho_{\mu\nu}$ is symmetric under interchange of μ and ν , its corresponding torsion vanishes. The curvature of a connection is given by the Riemann tensor defined as

$$R^\rho_{\sigma\mu\nu} = \partial_\mu \Gamma^\rho_{\nu\sigma} - \partial_\nu \Gamma^\rho_{\mu\sigma} + \Gamma^\rho_{\mu\lambda} \Gamma^\lambda_{\nu\sigma} - \Gamma^\rho_{\nu\lambda} \Gamma^\lambda_{\mu\sigma}. \quad (23)$$

From the Riemann tensor, we can obtain two more geometric quantities, the Ricci tensor defined as $R_{\mu\nu} = R^\sigma_{\mu\sigma\nu}$ and the Ricci scalar defined as $R = R^\mu_{\mu}$.

In terms of the full connection $\Gamma^\alpha_{\mu\nu} = \tilde{\Gamma}^\alpha_{\mu\nu} + K^\rho_{\mu\nu}$ the Riemann tensor is given by

$$R^\rho_{\sigma\mu\nu} = \tilde{R}^\rho_{\sigma\mu\nu} + 2\partial_{[\mu} K^\rho_{\nu]\sigma} + 2\tilde{\Gamma}^\rho_{[\mu|\lambda} K^\lambda_{\nu]\sigma} + 2K^\rho_{[\mu|\lambda} \tilde{\Gamma}^\lambda_{\nu]\sigma} + 2K^\rho_{[\mu|\lambda} K^\lambda_{\nu]\sigma}, \quad (24)$$

where $\tilde{R}^\rho_{\sigma\mu\nu}$ is defined equivalently to $R^\rho_{\sigma\mu\nu}$ in (23), but with $\Gamma^\alpha_{\beta\mu}$ replaced with $\tilde{\Gamma}^\alpha_{\beta\mu}$. The bracket notation $A_{[\mu|\nu} B_{\rho]}$ for example denotes anti-symmetrisation over only μ and ρ , leaving ν alone. The corresponding Ricci scalar is given by

$$R = \tilde{R} - K_{\rho\mu\nu} K^{\rho\mu\nu}, \quad (25)$$

where we have assumed that the contortion is completely anti-symmetric. We shall employ this simple formula in order to determine the curvature of the spaces we consider.

B. Spinor Fields on Riemann-Cartan Geometry

1. The Dirac Action

The action for a spin- $\frac{1}{2}$ particle of mass m defined on a general (2+1)-dimensional Riemann-Cartan spacetime M is given by⁵⁶

$$S_{\text{RC}} = \frac{i}{2} \int_M d^{2+1}x |e| (\bar{\psi} \gamma^\mu D_\mu - \overline{D_\mu \psi} \gamma^\mu \psi + 2im \bar{\psi} \psi), \quad (26)$$

where $\{\gamma^\mu\}$ are the *curved* space gamma matrices. These matrices obey the Clifford algebra $\{\gamma^\mu, \gamma^\nu\} = 2g^{\mu\nu}$ and are related to the flat space gamma matrices $\{\gamma^a\}$ via $\gamma^\mu = e_a^\mu \gamma^a$, which obey the flat space Clifford algebra $\{\gamma^a, \gamma^b\} = 2\eta^{ab}$. The gamma matrices obey $(\gamma^a)^\dagger = \gamma^0 \gamma^a \gamma^0$. The object $|e| = |\det[e^a_\mu]|$ which from (14) obeys $|e| = \sqrt{|g|}$, where g is the determinant of the metric. Using the flat space gamma matrices, we define the *Dirac adjoint* $\bar{\psi} = \psi^\dagger \gamma^0$.

The covariant derivative of spinors is given by

$$D_\mu \psi = \partial_\mu \psi + \omega_\mu \psi, \quad (27)$$

$$\overline{D_\mu \psi} = (D_\mu \psi)^\dagger \gamma^0 = \partial_\mu \bar{\psi} - \bar{\psi} \omega_\mu, \quad (28)$$

where ω_μ is given by

$$\omega_\mu = \frac{i}{2} \omega_{\mu ab} \Sigma^{ab}, \quad \Sigma^{ab} = \frac{i}{4} [\gamma^a, \gamma^b], \quad (29)$$

and $\omega_{\mu ab} = \eta_{ac} \omega^c_{\mu b}$ are the components of the spin connection. The operators $\{\Sigma^{ab}\}$ are the generators of the Lorentz algebra $\mathfrak{so}(2,1)$. We use the notation D_μ instead of ∇_μ to highlight the fact these derivatives are acting on spinors and not tensors. In this paper we shall refer to ω_μ as the connection as well.

Referring back to (21), we can expand out the connection as $\omega_\mu = \tilde{\omega}_\mu + K_\mu$, which means we can write

the covariant derivative as $D_\mu\psi = \tilde{D}_\mu\psi + K_\mu\psi$, where \tilde{D}_μ is the covariant derivative with respect to the Levi-Civita connection only. Using this and the fact that for a Levi-Civita connection Stokes' theorem yields the curved space analogue of the divergence theorem, we can integrate the action by parts to yield

$$S_{\text{RC}} = \int_M d^{2+1}x|e| \left(i\bar{\psi}\gamma^\mu\tilde{D}_\mu\psi + \frac{i}{2}\bar{\psi}\{\gamma^\mu, K_\mu\}\psi - m\bar{\psi}\psi \right), \quad (30)$$

where we have used $\tilde{D}_\mu\gamma^\mu = \tilde{D}_\mu e_a^\mu \gamma^a = 0$ for a metric compatible connection and ignored the boundary term. The object $\{\cdot, \cdot\}$ is the anti-commutator. This result can also be obtained by using the fact that $\partial_\mu(|e|e_a^\mu) = |e|\tilde{\omega}_{ab}^b$ so one can integrate by parts using partial derivatives in the usual sense.

Now, with the action in the form (30), we expand out the covariant derivative explicitly as $\tilde{D}_\mu\psi = \partial_\mu\psi + \tilde{\omega}_\mu\psi$ to yield

$$S_{\text{RC}} = \int_M d^{2+1}x|e| \left(i\bar{\psi}\gamma^\mu\partial_\mu\psi + i\bar{\psi}\gamma^\mu\tilde{\omega}_\mu\psi + \frac{i}{2}\bar{\psi}\{\gamma^\mu, K_\mu\}\psi - m\bar{\psi}\psi \right). \quad (31)$$

In order to simplify this action, we use the identities

$$\{\gamma^a, [\gamma^b, \gamma^c]\} = 4\epsilon^{abc}\gamma^0\gamma^1\gamma^2, \quad (32)$$

$$[\gamma^a, [\gamma^b, \gamma^c]] = -4(\gamma^b\eta^{ac} - \gamma^c\eta^{ab}), \quad (33)$$

of which the first holds only in (2+1)-dimensional space, where ϵ^{abc} is the totally anti-symmetric Levi-Civita *symbol*. This allows us to simplify the second term in the integrand of (31) giving

$$\begin{aligned} \gamma^\mu\tilde{\omega}_\mu &= \frac{1}{2}(\{\gamma^\mu, \tilde{\omega}_\mu\} + [\gamma^\mu, \tilde{\omega}_\mu]) \\ &= -\frac{1}{4}\tilde{\omega}_{abc}\epsilon^{abc}\gamma^0\gamma^1\gamma^2 + \frac{1}{2}\omega_{ab}^b\gamma^a. \end{aligned} \quad (34)$$

Using the definition of the contortion (18), the third term in the integrand of (31) is given by

$$\{\gamma^\mu, K_\mu\} = -\frac{1}{4}T_{abc}\epsilon^{abc}\gamma^0\gamma^1\gamma^2, \quad (35)$$

where we have used the definition of the contortion tensor (18). This demonstrates that the spinor only couples to the completely anti-symmetric part of the torsion T . So without loss of generality we can restrict our torsion to be completely anti-symmetric of the form

$$T_{abc} = \frac{1}{3!}\phi\epsilon_{abc}, \quad (36)$$

with corresponding contortion $K_{abc} = \frac{1}{12}\phi\epsilon_{abc}$, where ϕ is some pseudoscalar field. With this form of the torsion we have

$$\{\gamma^\mu, K_\mu\} = -\frac{1}{4}\phi\gamma^0\gamma^1\gamma^2. \quad (37)$$

Substituting these results into the action (31) gives the final form

$$\begin{aligned} S_{\text{RC}} = \int_M d^{2+1}x|e|\bar{\psi} &\left(ie_a^\mu\gamma^a\partial_\mu - \frac{i}{4}\tilde{\omega}_{abc}\epsilon^{abc}\gamma^0\gamma^1\gamma^2 \right. \\ &\left. + \frac{i}{2}\tilde{\omega}_{ab}^b\gamma^a - \frac{i}{8}\phi\gamma^0\gamma^1\gamma^2 - m \right)\psi. \end{aligned} \quad (38)$$

2. The Hamiltonian

We restrict our spacetime M to be a static spacetime of the form

$$M = \mathbb{R} \times \Sigma \quad (39)$$

with the natural coordinate system (t, x^i) , where \mathbb{R} corresponds to time and Σ is a two-dimensional curved space. In this way, we are assuming that only the purely spatial part of spacetime is curved and time can be viewed as a parameter. This is the case that corresponds to the geometric description of KHLM as time remains unaffected by the distortion of the system's couplings. The metric tensor for M takes the form $g = g_1 \oplus g_2$, where g_1 is the metric on \mathbb{R} and g_2 is the metric on Σ . The metric therefore takes a block-diagonal form in the natural coordinate system

$$g_{\mu\nu} = \begin{pmatrix} 1 & 0 & 0 \\ 0 & g_{xx} & g_{xy} \\ 0 & g_{xy} & g_{yy} \end{pmatrix} \quad (40)$$

and will be a constant in coordinate time, $\partial_t g_{\mu\nu} = 0$. The dreibein that correspond to this metric therefore take the form

$$e^a_\mu = \begin{pmatrix} 1 & 0 & 0 \\ 0 & e^1_x & e^1_y \\ 0 & e^2_x & e^2_y \end{pmatrix}, \quad e_a^\mu = \begin{pmatrix} 1 & 0 & 0 \\ 0 & e_{1x} & e_{1y} \\ 0 & e_{2x} & e_{2y} \end{pmatrix}. \quad (41)$$

where the convention taken is that the index a runs down the columns while the index μ runs along the rows. Using the definition (17), we see that any time components of the Levi-Civita connection $\tilde{\Gamma}^\rho_{\mu\nu}$ will vanish: $\tilde{\Gamma}^t_{\mu\nu} = \tilde{\Gamma}^\rho_{t\nu} = \tilde{\Gamma}^\rho_{\nu t} = 0$. This in turn imposes the constraint on the corresponding Levi-Civita spin connection: $\tilde{\omega}_{tb}^a = \tilde{\omega}_{\mu b}^a = \tilde{\omega}_{\mu 0}^a = 0$, while the contortion of the spin connection remains unaffected. Hence, for these configurations of the metric, the action (38) reduces to

$$\begin{aligned} S_{\text{RC}} = \int_M d^{2+1}x|e|\bar{\psi} &\left[ie_0^t\gamma^0\partial_t + ie_a^i\gamma^a \left(\partial_i + \frac{1}{2}\tilde{\omega}_{ib}^b \right) \right. \\ &\left. - \frac{i}{8}\phi\gamma^0\gamma^1\gamma^2 - m \right]\psi. \end{aligned} \quad (42)$$

We define the corresponding Lagrangian \mathcal{L}_{RC} via $S_{\text{RC}} = \int_M d^{2+1}x|e|\mathcal{L}_{\text{RC}}$, where we stress that the determinant $|e|$ is part of the integration measure $d^{2+1}x|e|$.

As we have assumed our spacetime is static, we can define the Hamiltonian density from the Lagrangian density \mathcal{L}_{RC} via a Legendre transformation:

$$\mathcal{H}_{\text{RC}} = \frac{\partial \mathcal{L}_{\text{RC}}}{\partial \dot{\psi}} \dot{\psi} + \dot{\psi} \frac{\partial \mathcal{L}_{\text{RC}}}{\partial \dot{\psi}} - \mathcal{L}_{\text{RC}} \quad (43)$$

where $\dot{\psi} \equiv \partial_t \psi$. The Hamiltonian density is given by

$$\mathcal{H}_{\text{RC}} = \bar{\psi} \left[-ie_a^i \gamma^a \left(\partial_i + \frac{1}{2} \tilde{\omega}_{ib}^b \right) + \frac{i}{8} \phi \gamma^0 \gamma^1 \gamma^2 + m \right] \psi. \quad (44)$$

As the metric and dreibein are in the form (40) and (41), the integration measure on Σ is given by $d^2x \sqrt{|g_2|} = d^2x |e|$, where g_2 is the metric on Σ . We therefore define the Hamiltonian by $H_{\text{RC}} = \int_{\Sigma} d^2x |e| \mathcal{H}_{\text{RC}} \equiv \int_{\Sigma} d^2x |e| \psi^\dagger h_{\text{RC}} \psi$, where h_{RC} is the *single-particle* Hamiltonian given by

$$h_{\text{RC}} = e_a^i \gamma^0 \gamma^a p_i + \frac{i}{8} \phi \gamma^1 \gamma^2 + m \gamma^0, \quad (45)$$

which is an operator on the Hilbert space of single-particle spinor wave functions and the Hermitian canonical momentum operator is defined as

$$p_\mu = -i \left(\partial_\mu + \frac{1}{2} \tilde{\omega}_{\mu a}^a \right). \quad (46)$$

The hermiticity of p_μ and Hamiltonian h_{RC} is discussed in appendix A. The Hamiltonian H_{RC} is what we identify as the *many-body Hamiltonian* of the Riemann-Cartan theory.

IV. RIEMANN-CARTAN GEOMETRY FROM THE KITAEV HONEYCOMB LATTICE MODEL

We will now deform the original Kitaev model by varying its couplings in order to obtain a Riemann-Cartan Hamiltonian as given by (45). There are several aspects of this Hamiltonian that we would like to identify in the continuous limit of the KHLM. In particular, we have the non-trivial geometry encoded in the gamma matrices through the dreibein $\{e_a^\mu\}$ as well as the spin connection $\tilde{\omega}_{\mu b}^a$. Moreover, the torsion field ϕ , as well as the mass m , have their own terms in the Hamiltonian. In order for these terms to emerge, they require corresponding terms in the microscopic lattice model.

Before comparing the continuum limit of the honeycomb model with a Riemann-Cartan field theory, it is important to be aware of the following. The many-body Hamiltonian of the continuum limit of Kitaev's honeycomb model expressed in position space is given by

$$H_{\text{KHLM}} = \int d^2x \Psi^\dagger h_{\text{KHLM}} \Psi, \quad (47)$$

while the many-body Hamiltonian obtained from the Riemann-Cartan field theory is given by

$$H_{\text{RC}} = \int_{\Sigma} d^2x |e| \psi^\dagger h_{\text{RC}} \psi. \quad (48)$$

Note that these many-body Hamiltonians differ by a factor of the determinant $|e|$ within the integrands. If we wish to interpret the continuum limit of the lattice model as a Riemann-Cartan theory by directly comparing these Hamiltonians, we must use the correct integration measure $d^2x |e|$ and *not* d^2x alone. Consequently, we see that any *single-particle* Hamiltonian describing the continuum limit of the lattice model will have a factor of the determinant $|e|$ absorbed into it, in other words $h_{\text{KHLM}} = |e| h_{\text{RC}}$ and $\Psi = \psi$.

In order to achieve a non-trivial curvature and torsion, we require a metric that has space-dependent components which therefore requires a model with space dependent parameters $\{J_i\}$ and K . In this section, we shall assume that the continuum limit of the model with space-dependent parameters takes the same form as the model with constant parameters, but with the parameters simply upgraded to being slowly varying space-dependent functions.

A. The isotropic $J_x = J_y = J_z = J$ case

We first focus on the homogeneous coupling case for which $J_x = J_y = J_z = J$ and we interpret it as a Riemann-Cartan theory. We identify the dreibein, metric, connection, curvature and torsion of the model.

1. The Metric

Taking into account that $h_{\text{KHLM}} = |e| h_{\text{RC}}$, a direct comparison of the isotropic continuum limit (12) with the Riemann-Cartan Hamiltonian (45) reveals that

$$|e| e_1^x = 3J, \quad |e| e_2^y = -3J. \quad (49)$$

If we assume that the dreibein e_a^μ are diagonal

$$e_a^\mu = \begin{pmatrix} 1 & 0 & 0 \\ 0 & e_1^x & 0 \\ 0 & 0 & e_2^y \end{pmatrix}, \quad e^a_\mu = \begin{pmatrix} 1 & 0 & 0 \\ 0 & \frac{1}{e_1^x} & 0 \\ 0 & 0 & \frac{1}{e_2^y} \end{pmatrix}, \quad (50)$$

we have $|e| = |\det[e_a^\mu]| = \frac{1}{|e_1^x| |e_2^y|}$. Solving the equations reveals $e_1^x = \frac{1}{3J}$ and $e_2^y = -\frac{1}{3J}$ and thus $|e| = 9J^2$. From this, we find the metric is given by

$$g_{\mu\nu} = e^a_\mu e^b_\nu \eta_{ab} = \begin{pmatrix} 1 & 0 & 0 \\ 0 & -9J^2 & 0 \\ 0 & 0 & -9J^2 \end{pmatrix}. \quad (51)$$

2. Curvature and Torsion

As presented previously, the curvature and torsion of a spacetime depends upon which connection we are working with. As we are working on a static spacetime of the

form $M = \mathbb{R} \times \Sigma$, the metric, after diagonalisation, takes the form

$$g_{\mu\nu} = \begin{pmatrix} 1 & 0 & 0 \\ 0 & F & 0 \\ 0 & 0 & G \end{pmatrix}, \quad (52)$$

where $F = F(x, y)$ and $G = G(x, y)$ are arbitrary functions of space only. A metric of this form yields the Levi-Civita connection $\tilde{\Gamma}_{\mu\nu}^\alpha = \frac{1}{2}g^{\alpha\beta}(\partial_\mu g_{\beta\nu} + \partial_\nu g_{\beta\mu} - \partial_\beta g_{\mu\nu})$, where

$$\begin{aligned} \tilde{\Gamma}_{xx}^x &= \frac{1}{2F}\partial_x F, & \tilde{\Gamma}_{xy}^x &= \tilde{\Gamma}_{yx}^x = \frac{1}{2F}\partial_y F, \\ \tilde{\Gamma}_{yy}^x &= -\frac{1}{2F}\partial_x G, & \tilde{\Gamma}_{yy}^y &= \frac{1}{2G}\partial_y G, \\ \tilde{\Gamma}_{xy}^y &= \tilde{\Gamma}_{yx}^y = \frac{1}{2G}\partial_x G, & \tilde{\Gamma}_{xx}^y &= -\frac{1}{2G}\partial_y F, \end{aligned} \quad (53)$$

while all time components vanish.

We first calculate the curvature of the Levi-Civita connection. As all of the time components of the Levi-Civita connection vanish, so will all of the time components of its corresponding curvature. For this reason, we can restrict ourselves to the two-dimensional spatial hypersurface Σ . It easily shown that the Riemann tensor in a two-dimensional space has only one independent component and is of the form

$$\tilde{R}_{ijkl} = \frac{1}{2}\tilde{R}(g_{ik}g_{lk} - g_{il}g_{kj}), \quad (54)$$

where \tilde{R} is the Ricci scalar and i, j, k, \dots denote spatial components. With a metric in the form (52), giving the connection (53), we find the corresponding Ricci scalar is given by

$$\tilde{R} = -\frac{1}{2}\left[\partial_x\left(\frac{\partial_x G}{FG}\right) + \partial_y\left(\frac{\partial_y F}{FG}\right) + \frac{\partial_x^2 G + \partial_y^2 F}{FG}\right] \quad (55)$$

and hence the Riemann tensor is fully determined.

For the isotropic case we have $F = G = -9J^2$. Employing (55) we obtain the Ricci scalar to be given by the simple formula

$$\tilde{R} = -2\partial^2 \ln J, \quad (56)$$

where $\partial^2 = g^{\mu\nu}\partial_\mu\partial_\nu$ is the Laplacian operator. Hence, in order to obtain non-zero curvature from the Levi-Civita connection the J -couplings of the KHLM need to be position dependent. In particular when $\partial_i J = 0$, then $\tilde{R} = 0$.

For the isotropic case, comparison of (12) with (45) also reveals that $|e|^{\frac{\phi}{8}} = -3\sqrt{3}K$, with $|e| = 9J^2$, which gives us

$$\phi = -\frac{8\sqrt{3}K}{3J^2} \quad (57)$$

and hence the torsion and contortion are given by

$$T_{\mu\nu\sigma} = -\frac{4\sqrt{3}K}{9J^2}\epsilon_{\mu\nu\sigma}, \quad K_{\mu\nu\sigma} = -\frac{2\sqrt{3}K}{9J^2}\epsilon_{\mu\nu\sigma}. \quad (58)$$

that finally give

$$K_{\rho\mu\nu}K^{\rho\mu\nu} = \left(\frac{2}{9}\right)^3 \frac{K^2}{J^8}. \quad (59)$$

Hence, we can now determine the total curvature (25) given explicitly in terms of the couplings of the lattice model

$$R = -2\partial^2 \ln J - \left(\frac{2}{9}\right)^3 \frac{K^2}{J^8}. \quad (60)$$

Note that the total curvature R is non-zero even when $\partial_i J = 0$, due to the contribution from the torsion ϕ .

By comparing the continuum limit of KHLM Hamiltonian (17) with the corresponding Hamiltonian of the Majorana field in Riemann-Cartan geometry (45), we observe that $m = 0$. In other words, the KHLM corresponds to *massless* Majoranas. Hence, the energy gap of the KHLM comes from the non-zero torsion field and not the mass of the Majorana fermions. As seen in (58) the torsion in the KHLM emerges from the next-to-nearest neighbour K -coupling terms in the Majorana representation of the model which itself is derived from the three spin interactions, as given in (1). These interactions were inserted in the KHLM to generate an energy gap in order to give rise to a well defined non-Abelian topological phase.

3. Mass from Kekulé distortion

The energy gap of the original Kitaev model comes from the K term that is equivalent to torsion in the continuum limit. To give rise to a mass term in the continuum limit, we need to introduce a Kekulé distortion in the tunnelling couplings of the Majorana fermions. This method is similar to the one employed in graphene to theoretically generate a mass gap⁵⁸ and adjusted further to the case of Majorana fermions⁴⁹.

To proceed we consider an additional term in the lattice Hamiltonian of the Kitaev honeycomb lattice model of the form

$$\delta H = i \sum_{i \in A} \sum_{k=1}^3 \delta J_{ik} c_{\mathbf{r}_i}^a c_{\mathbf{r}_i + \mathbf{s}_k}^b + \text{h.c.}, \quad (61)$$

where A is the sub-lattice defined in Fig. 1 and the vectors \mathbf{s}_1 , \mathbf{s}_2 and \mathbf{s}_3 are defined in Fig. 3. With this term the couplings J_x , J_y and J_z that were taken to be equal and homogeneous before, are now distorted in the following way

$$\delta J_{ik} = \frac{m}{3} e^{i\mathbf{P}_+ \cdot \mathbf{s}_k} e^{i(\mathbf{P}_+ - \mathbf{P}_-) \cdot \mathbf{r}_i} + \text{c.c.} \quad (62)$$

with m a real constant number. This additional term causes a Kekulé distortion in the couplings of the honeycomb lattice that has the form shown in Fig. 3.

The Kekulé distortion changes the unit cell of the honeycomb lattice to include six sites, causing the Brillouin

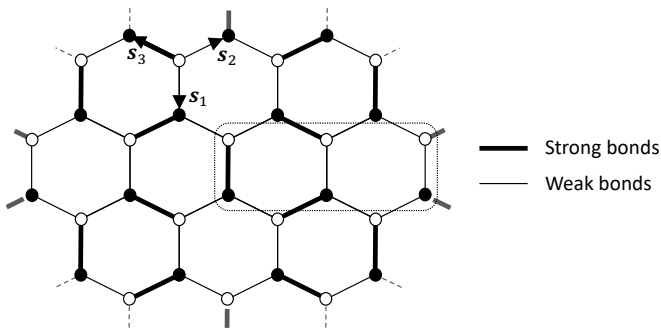


FIG. 3. The Kekulé distortion in the couplings of the honeycomb lattice model, as described by Eqns. (61) and (62), which generate a mass term in the Hamiltonian. Strong and weak tunnelling couplings are indicated as thick and thin bonds, respectively, between lattice sites. This configuration of couplings is periodic with respect to a unit cell with six sites, as shown. The vectors $\mathbf{s}_1 = (0, -1)$, $\mathbf{s}_2 = (\frac{\sqrt{3}}{2}, \frac{1}{2})$, $\mathbf{s}_3 = (-\frac{\sqrt{3}}{2}, \frac{1}{2})$ used in (62) translate between lattices A and B are also depicted.

zone to fold three times compared to the undisturbed case. Subsequently, we Fourier transform and restrict ourselves to the low energy contributions near the Fermi points. Up to linear order in momenta the additional term, δH , gives the following contribution around the Fermi points⁴⁹

$$\delta H = \Psi^\dagger \gamma^0 m \Psi. \quad (63)$$

The contribution to the single-particle Hamiltonian is therefore

$$h_m = m \gamma^0, \quad (64)$$

where $\gamma^0 = \sigma^x \otimes \mathbb{I}$, which is the mass term given in (45). Hence, the Majorana fermions in the continuum limit of the KHLM can acquire a mass if a non-trivial Kekulé distortion is inserted.

When $K = 0$ the Kekulé distortion creates an energy gap due to a non-zero mass m . In this situation vertices of sub-lattice A are coupled exclusively to vertices of sub-lattice B . So the KHLM recovers its chiral symmetry and the phase of the system belongs in the BDI class that has trivial Chern number⁵⁹. Nevertheless, zero dimensional defects, such as vortices, can trap chiral Majorana zero modes^{49,59,60}. This should be contrasted with the case where only the K -term is present and the model is equivalent to the $p+ip$ superconductor belonging to class D⁵⁹. By varying the couplings of the extended Kitaev model, it is possible to induce a phase transition between these two phases. The phase diagram of the model as m and K are varied is shown in Fig. 4.

B. The generally anisotropic J coupling case

We now turn away from the homogeneous coupling case $J_x = J_y = J_z$ and consider cases which yield a non-

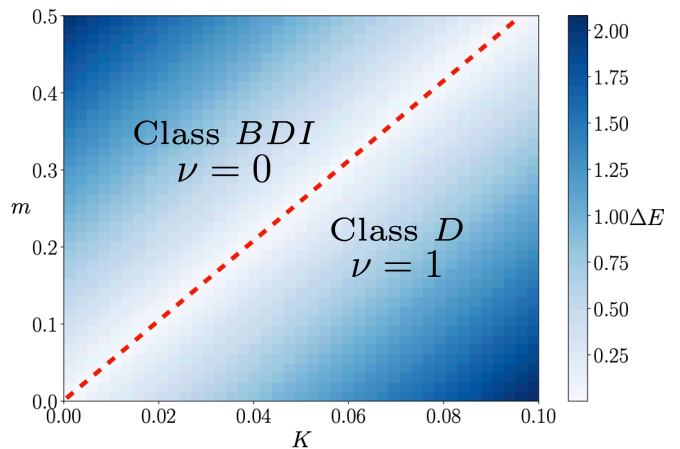


FIG. 4. Phase diagram of the KHLM with its energy gap ΔE varying as a function of the K coupling and the mass, m . By increasing the Kekulé distortion a phase transition is induced from the gapped topological phase of the KHLM with Chern number $\nu = 1$ that belongs in class D to a gapped Kekulé phase with Chern number $\nu = 0$ that belongs in class BDI. Both of these phases support vortices that bound Majorana zero modes. The red dashed line denotes the phase transition boundary.

trivial metric in the continuum limit. In particular, we consider the completely anisotropic case where all $\{J_i\}$ couplings are unequal. Moreover, we allow for anisotropy in the K -couplings taking values K_x , K_y and K_z depending on their orientation, as shown in Fig. 5, so as not to shift the Fermi points. In this case, the Kitaev model Hamiltonian takes the form $H = \int d^2q \psi_q^\dagger h(\mathbf{q}) \psi_q$, where $\psi_q = (c_q^a \ c_q^b)^\top$, and the single-particle Hamiltonian $h(\mathbf{q})$ given by

$$h(\mathbf{q}) = \begin{pmatrix} \Delta(\mathbf{q}) & -f(\mathbf{q}) \\ -f^*(\mathbf{q}) & -\Delta(\mathbf{q}) \end{pmatrix}, \quad (65)$$

where

$$f(\mathbf{q}) = 2(J^x e^{i\mathbf{q} \cdot \mathbf{n}_1} + J^y e^{i\mathbf{q} \cdot \mathbf{n}_2} + J^z), \quad (66)$$

and

$$\Delta(\mathbf{q}) = 2[-K_x \sin(\mathbf{q} \cdot \mathbf{n}_1) + K_y \sin(\mathbf{q} \cdot \mathbf{n}_2) + K_z \sin(\mathbf{q} \cdot (\mathbf{n}_1 - \mathbf{n}_2))]. \quad (67)$$

Next, we consider the continuum limit of Hamiltonian (65).

For $K_i = 0$ we expect the system to have Fermi points. We first determine these points for the most general configuration of $\{J_i\}$ couplings. Following the procedure we employed in the isotropic case, we solve for the momenta $\mathbf{q} = \mathbf{P}$ such that $f(\mathbf{P}) = 0$. This condition gives two equations

$$J_x \cos(\mathbf{P} \cdot \mathbf{n}_1) + J_y \cos(\mathbf{P} \cdot \mathbf{n}_2) + J_z = 0, \quad (68)$$

$$J_x \sin(\mathbf{P} \cdot \mathbf{n}_1) + J_y \sin(\mathbf{P} \cdot \mathbf{n}_2) = 0. \quad (69)$$

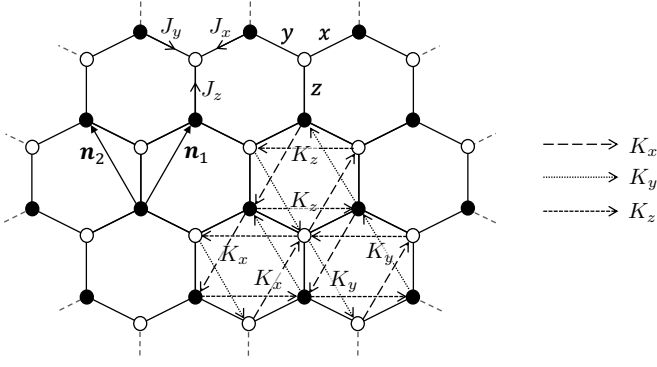


FIG. 5. The anisotropic KHLM is given by choosing the couplings J_x , J_y and J_z to be unequal, giving rise to an anisotropic model. In order to have the K -term contribute purely an energy gap we choose the couplings K_x , K_y and K_z to be also anisotropic and functions of J_i 's, as given by (75).

There are two solutions to these equations corresponding to two Fermi points located at momenta

$$\mathbf{P}_{\pm} = \pm \left(\begin{array}{c} \frac{1}{\sqrt{3}}(\arccos(a) + \arccos(b)) \\ \frac{1}{3}(\arccos(a) - \arccos(b)) \end{array} \right), \quad (70)$$

where

$$a = \frac{J_y^2 - J_x^2 - J_z^2}{2J_x J_z} \quad \text{and} \quad b = \frac{J_x^2 - J_y^2 - J_z^2}{2J_y J_z}. \quad (71)$$

To determine the behaviour of the Hamiltonian around these points, we Taylor expand to first order as

$$\begin{aligned} f(\mathbf{P}_{\pm} + \mathbf{p}) &= f(\mathbf{P}_{\pm}) + \mathbf{p} \cdot \nabla f(\mathbf{P}_{\pm}) + O(p^2), \\ \Delta(\mathbf{P}_{\pm} + \mathbf{p}) &= \Delta(\mathbf{P}_{\pm}) + \mathbf{p} \cdot \nabla \Delta(\mathbf{P}_{\pm}) + O(p^2). \end{aligned} \quad (72)$$

By direct calculation we find

$$\begin{aligned} \nabla f(\mathbf{P}_{\pm}) &= 2i[J_x(a \pm i\sqrt{1-a^2})\mathbf{n}_1 + \\ &\quad J_y(b \mp i\sqrt{1-b^2})\mathbf{n}_2], \end{aligned} \quad (73)$$

and

$$\begin{aligned} \nabla \Delta(\mathbf{P}_{\pm}) &= 2 \left[-K_x a \mathbf{n}_1 + K_y b \mathbf{n}_2 \right. \\ &\quad \left. + K_z \left(ab - \sqrt{1-a^2}\sqrt{1-b^2} \right) (\mathbf{n}_1 - \mathbf{n}_2) \right]. \end{aligned} \quad (74)$$

For the isotropic case addressed earlier in section IV A, we note that in the continuum limit $f(\mathbf{p})$ became the kinetic term whilst $\Delta(\mathbf{p})$ served to provide an energy gap at the Fermi points. If we demand that this is the case for inhomogeneous couplings, we must ensure that $\Delta(\mathbf{p})$ does not shift the position of the Fermi points which can be achieved if (74) vanishes. In order to impose this, we must constrain the $\{K_i\}$ couplings to take the values

$$\begin{aligned} K_x &= 4Kb \left(ab - \sqrt{1-a^2}\sqrt{1-b^2} \right), \\ K_y &= 4Ka \left(ab - \sqrt{1-a^2}\sqrt{1-b^2} \right), \\ K_z &= 4Kab, \end{aligned} \quad (75)$$

where $K \in \mathbb{R}$ is a constant that gives the overall scale of the K -couplings and a, b are given in (71). The factor of 4 ensures the gap for the most general case agrees with the gap from the isotropic case in Section II. With these conditions, the energy gap at each Fermi point is given by $\Delta(\mathbf{P}_{\pm}) = \pm\Delta$, where

$$\Delta = 8K\sqrt{(1-a^2)(1-b^2)}(a\sqrt{1-b^2} + b\sqrt{1-a^2}). \quad (76)$$

At the isotropic limit, $J_x = J_y = J_z = J$, we have from (71) that $a = b = -J/2$ and we recover the corresponding gap $\Delta = 3\sqrt{3}K$, in agreement with (9).

As usual, we expand our Hamiltonian about the Fermi points and define the continuum limit Hamiltonian as $h_{\pm}(\mathbf{p}) = h(\mathbf{P}_{\pm} + \mathbf{p})$. We next consider the Fermi points simultaneously by defining the four component spinor $\Psi = (c_+^a \quad ic_+^b \quad ic_-^b \quad c_-^a)^T$ and combining the Hamiltonians $h_+(\mathbf{p})$ and $h_-(\mathbf{p})$ by taking the direct sum with respect to the basis defined by Ψ . This yields the total Hamiltonian

$$\begin{aligned} h_{\text{KHLM}} &= (A\sigma^z \otimes \sigma^x + B\sigma^z \otimes \sigma^y)p_x \\ &\quad + C\sigma^z \otimes \sigma^y p_y + \Delta \mathbb{I} \otimes \sigma^z, \end{aligned} \quad (77)$$

where we have defined the quantities

$$A = \sqrt{12J_x^2 - 3\frac{(J_y^2 - J_x^2 - J_z^2)^2}{J_z^2}}, \quad (78)$$

$$B = \sqrt{3}\frac{(J_y^2 - J_x^2)}{J_z^2}, \quad (79)$$

$$C = -3J_z. \quad (80)$$

This reduces to the original homogeneous continuum limit given in (9) when $J_x = J_y = J_z = J$. In terms of the gamma matrices, we see that the continuum limit Hamiltonian is given by

$$h_{\text{KHLM}} = (A\gamma^0\gamma^1 + B\gamma^0\gamma^2)p_x + C\gamma^0\gamma^2 p_y + i\Delta\gamma^1\gamma^2, \quad (81)$$

while the corresponding Riemann-Cartan Hamiltonian is

$$h_{\text{RC}} = e_a^i \gamma^0 \gamma^a p_i + \frac{i}{8} \phi \gamma^1 \gamma^2 + m\gamma^0. \quad (82)$$

Direct comparison, with the identification that $h_{\text{KHLM}} = |e|h_{\text{RC}}$ yields the equations

$$|e|e_1^x = A, \quad |e|e_2^x = B, \quad |e|e_2^y = C, \quad \frac{|e|\phi}{8} = \Delta. \quad (83)$$

We take our dreibein to be of the form

$$e_a^{\mu} = \begin{pmatrix} 1 & 0 & 0 \\ 0 & e_1^x & 0 \\ 0 & e_2^x & e_2^y \end{pmatrix}, \quad e^a_{\mu} = \begin{pmatrix} 1 & 0 & 0 \\ 0 & \frac{1}{e_1^x} & 0 \\ 0 & -\frac{e_2^x}{e_1^x e_2^y} & \frac{1}{e_2^y} \end{pmatrix} \quad (84)$$

In this case, the determinant is given by

$$|e| = |\det[e^a_{\mu}]| = \frac{1}{|e_1^x| |e_2^y|}. \quad (85)$$

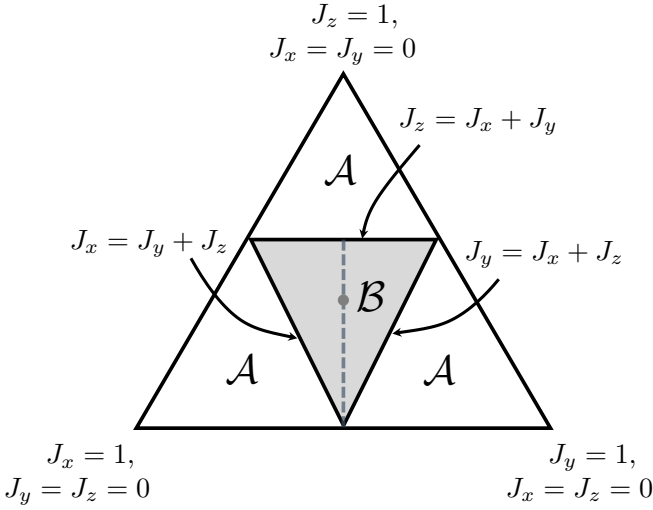


FIG. 6. The phase diagram of the anisotropic KHLM, where the couplings are normalised as $J_x + J_y + J_z = 1$. The isotropic case with $J_x = J_y = J_z$ is denoted by a dot in the centre of the triangles. The quantum spin liquid phase that supports Majorana fermions, denoted as \mathcal{B} , sits in the centre of the diagram. The topological phases \mathcal{A} correspond to the Toric Code phase. The singularity condition of the metric (89) defines the boundaries between the phases \mathcal{A} and \mathcal{B} . The dashed line corresponds to a possible anisotropic change of couplings in the \mathcal{B} phase.

With this, solving equations (83) yields the dreibein

$$e_a^\mu = \begin{pmatrix} 1 & 0 & 0 \\ 0 & -\frac{1}{C} & 0 \\ 0 & -\frac{B}{AC} & -\frac{1}{A} \end{pmatrix}, \quad e^a_\mu = \begin{pmatrix} 1 & 0 & 0 \\ 0 & -C & 0 \\ 0 & B & -A \end{pmatrix}. \quad (86)$$

with $|e| = |A||C|$. From this expression, we can calculate the metric

$$g_{\mu\nu} = e^a_\mu e^b_\nu \eta_{ab} = \begin{pmatrix} 1 & 0 & 0 \\ 0 & -(B^2 + C^2) & AB \\ 0 & AB & -A^2 \end{pmatrix}. \quad (87)$$

Combining the result (86) with the fourth equation of (83), we see that the torsion pseudoscalar ϕ of the model is given by

$$\phi = \frac{8\Delta}{|A||C|}. \quad (88)$$

From (86) and (88) we see that the geometry becomes singular when $A = 0$ or $C = 0$. To analyse the properties of the model when $A = 0$ we note that this condition is equivalent to satisfying one of the following equations

$$\begin{aligned} J_x + J_y + J_z &= 0, \\ J_x - J_y - J_z &= 0, \\ J_x - J_y + J_z &= 0, \\ J_x + J_y - J_z &= 0. \end{aligned} \quad (89)$$

Assuming that J_x, J_y, J_z are all positive we obtain the following conditions $J_x = J_y + J_z$ or $J_y = J_x + J_z$ or

$J_z = J_x + J_y$. Choosing for convenience normalisation condition $J_x + J_y + J_z = 1$ we obtain the triangular phase diagram shown in Fig. 6. The above conditions between the J_i couplings define the phase boundaries that lie between the non-Abelian phase \mathcal{B} and the Toric Code³⁴ phases \mathcal{A} of the model. On the other hand, the condition $C = 0$ corresponds to the case where $J_z = 0$. This coupling configuration makes the model gapless as it becomes a set of disentangled one-dimensional chains with zero energy gap. The $J_z = 0$ case corresponds to the middle of the bottom site of the large triangle in Fig. 6. Hence, the geometric description of the KHLM is non-singular within the whole region \mathcal{B} . The singular regions of the metric correspond to the well known phase transitions of the KHLM³³.

C. The inhomogeneous case with $J_x = J_y = 1$ and $0 \leq J_z \leq 2$

The phase diagram obtained above corresponds to parameters $\{J_i\}$ that are constant. We now upgrade these parameters to functions of space to investigate whether the continuum limit can describe a *curved* geometry.

For simplicity, we focus our attention on the special anisotropic case where $J_x = J_y = 1$ and J_z can take values between the critical points $0 \leq J_z \leq 2$, as shown in Fig. 6. In this case, the metric reduces to

$$g_{\mu\nu} = \begin{pmatrix} 1 & 0 & 0 \\ 0 & -9J_z^2 & 0 \\ 0 & 0 & -3(4 - J_z^2) \end{pmatrix}. \quad (90)$$

As this metric is of the diagonal form (52) with $F = -9J_z^2$ and $G = 3(J_z^2 - 4)$, we can employ the Levi-Civita connection, $\tilde{\Gamma}_{\mu\nu}^\alpha$, given in (53) and the corresponding Ricci curvature given by (55). A direct substitution of F and G gives

$$\begin{aligned} \tilde{R} &= -\frac{2}{3(4 - J_z^2)^2} \left[\frac{1}{3}(\partial_x J_z)^2 - (\partial_y J_z)^2 \right] \\ &\quad - \frac{2}{3J_z(4 - J_z^2)} \left(\frac{1}{3}\partial_x^2 J_z - \partial_y^2 J_z \right). \end{aligned} \quad (91)$$

With the Ricci scalar \tilde{R} , together with the formula (54) we have fully determined the curvature of the Levi-Civita connection.

Next we determine the torsion of the system. Using equation (76) we find that the gap at the Fermi points is given by

$$\Delta = -K J_z (4 - J_z^2)^{\frac{3}{2}}. \quad (92)$$

Combining this result with the equation (88), we have

$$\phi = \frac{8\sqrt{3}}{9} K (J_z^2 - 4), \quad (93)$$

which fully determines our torsion $T_{\rho\mu\nu} = \frac{1}{3!}\phi\epsilon_{\rho\mu\nu}$ and contortion $K_{\rho\mu\nu} = \frac{1}{12}\phi\epsilon_{\rho\mu\nu}$ tensors. This result, combined with the Levi-Civita connection, fully determines

the spacetime connection $\Gamma_{\mu\nu}^\rho = \tilde{\Gamma}_{\mu\nu}^\rho + K_{\mu\nu}^\rho$ of the model. We can use the above results to determine the full curvature of the model that is given by

$$R = \tilde{R} + \left(\frac{2}{9}\right)^3 \frac{K^2(J_z^2 - 4)}{3J_z^2}, \quad (94)$$

with \tilde{R} given by (91). In the following section we shall investigate how faithfully KHLM can reproduce the metric (90) just by varying its couplings.

V. GEOMETRY OF QUANTUM CORRELATIONS AND ZERO MODES

In this section we perform a numerical study of the KHLM with periodic boundary conditions and anisotropic J couplings. Our aim is to determine how faithfully the exact form of the metric obtained in (90) can be reproduced from the lattice description of the microscopic model. To proceed we employ the following procedure. The geometric description of KHLM determines the form of the metric for any configuration of the couplings. By knowing for example an eigenstate of the Hamiltonian for a given configuration such as the isotropic, we can deduce the form of the eigenstate for any other coupling configuration by only considering its spatial transformation according to the corresponding change of the metric.

To be more concrete consider the transformation of the model from the isotropic case, $J_x = J_y = J_z = 1$, to the anisotropic case with $J_x = J_y = 1$ and $0 \leq J_z \leq 2$ described by the metric (90). As J_z varies this metric describes the simultaneous change in the measure of distance for both the x and y directions. To study systematically this effect we consider the case where J_z is constant in space. In this case the spatial distance d between two points on the the distorted space Σ is given by

$$d = \sqrt{-g_{ij} \Delta X^i \Delta X^j}, \quad (95)$$

where ΔX^i is the change in coordinates between each point and g_{ij} are the spatial components of the metric. We can visualise what the effect of changing the coupling J_z is on the spatial anisotropy by noting that a circle at $J_z = 1$ gets deformed into an ellipse as $J_z \neq 1$ with principle axes d_x and d_y along the x and y directions, respectively, satisfying

$$\frac{d_x}{d_y} = \frac{\sqrt{-g_{xx}}}{\sqrt{-g_{yy}}} = \frac{\sqrt{3}J_z}{\sqrt{4 - J_z^2}}. \quad (96)$$

In the following we study the effect varying J_z has on physical observables of the model. Specifically we will investigate how faithfully the two-point Majorana correlations and the shape of a Majorana zero mode³³, bounded at a vortex, are deformed compared to the ratio (96).

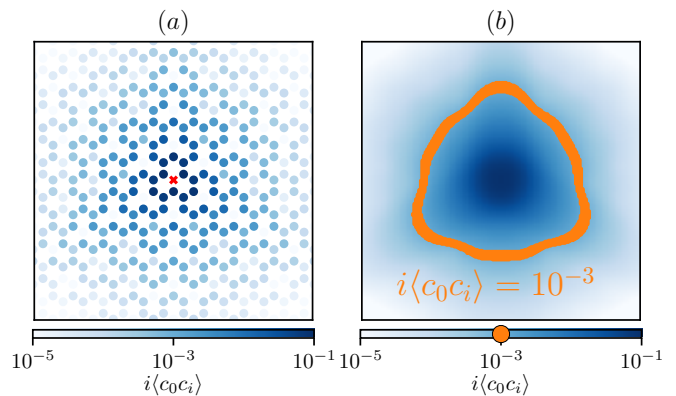


FIG. 7. The two-point correlations and their continuous profile. (a) The two-point correlations $i\langle c_0 c_i \rangle$ between each site, i and a central reference site, 0, denoted with a red cross. (b) A continuous approximation of the two-point correlations is constructed using two-dimensional Gaussians centred on each lattice site, as described by (97). The size and shape of the correlations are characterised by finding the set of points where $i\langle c_0 c_i \rangle = 10^{-3}$, as illustrated. We notice that even for large system sizes the hexagonal geometry of the lattice influences the spatial distribution of the correlations. Here we used $J_x = J_y = J_z = 1$, $K = 0.125$, $L = 36$ and $\epsilon = 1$.

A. Two-Point Quantum Correlations

Two-point Majorana correlations are the expectation value of a product of two Majorana operators at different sites with respect to the ground state $|\psi_0\rangle$, i.e. $i\langle c_i c_j \rangle = \langle \psi_0 | i c_i c_j | \psi_0 \rangle$. They are an important quantity as any other property of the model can be deduced from it as our model is effectively free⁶¹. As the system is gapped we expect the two-point correlations $i\langle c_i c_j \rangle$ to decrease exponentially fast with respect to the distance $|\mathbf{r}_i - \mathbf{r}_j|$. We extract the two-point correlations by exact diagonalisation of Hamiltonian (2).

We study the effect of varying J_z , as in Fig. 6, on the correlations of each site with respect to a central reference site, as shown in Fig. 7(a). We can produce a continuous approximation of these correlations by replacing each lattice point with a two-dimensional Gaussian centred at the site,

$$i\langle c(\mathbf{r}) c_j \rangle = \sum_i i\langle c_i c_j \rangle \delta(\mathbf{r} - \mathbf{r}_i) \rightarrow \sum_i \frac{i\langle c_i c_j \rangle}{2\pi\epsilon} e^{-\frac{|\mathbf{r} - \mathbf{r}_i|^2}{2\epsilon}}, \quad (97)$$

where ϵ is taken to be of similar magnitude as to the lattice spacing so that the Gaussians of neighbouring sites overlap. Fig. 7 illustrates this substitution. This continuous approximation reduces the discrete lattice effects and allows us extract the stretching and squeezing of the observables predicted by (96). It is worth noticing that as the two-point correlations are local they are strongly influenced by the lattice structure of the system. Hence, even if we expected the isotropic point to be rotationally invariant we observe that the honeycomb lattice structure

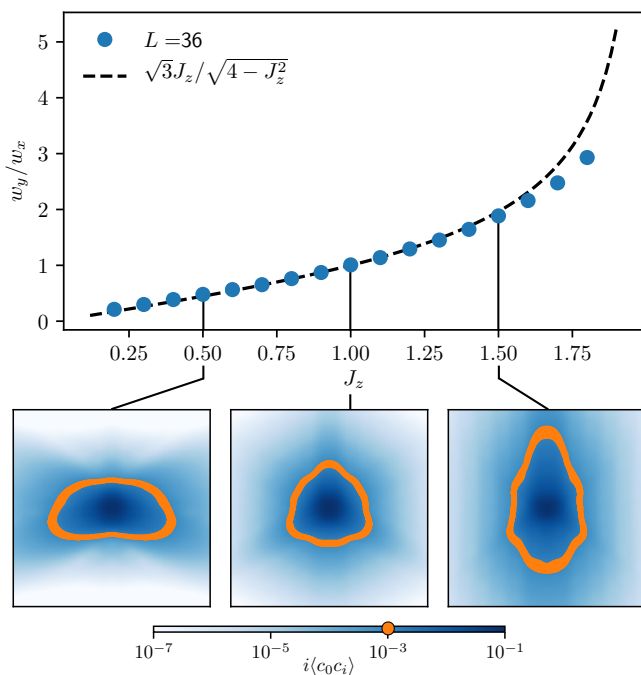


FIG. 8. Verifying the metric from the continuous approximation of the correlations. The dots in the main panel plot the ratio between the height and width of the ‘boundary’ w_y/w_x for $J_x = J_y = 1$, $K = 0.125$, $\epsilon = 1$ and system size 36×36 . Also plotted with a dashed line is the theoretically predicted ratio $d_x/d_y = \sqrt{3}J_z/\sqrt{4-J_z^2}$ from Eq. (96). Below are illustrative examples of the boundaries we find at various J_z . At the isotropic point, $J_z = 1$, we find $w_y/w_x = 1$. As J_z deviates from the isotropic point the ratio w_y/w_x can become larger or smaller than one.

is still evident in the continuum representation even for large system sizes. Nevertheless, this deformation does not obstruct us from demonstrating the equivalence between the microscopic model and the RC geometric theory.

From the continuous approximation of the correlations we numerically identify the set of points where $\langle c(\mathbf{r})c_j \rangle$ has decayed to a fixed value e.g. 10^{-3} . This ‘boundary’ line is drawn for the correlations at the isotropic point of the model in Fig. 7(b). We find that at the isotropic point the boundary is almost circular. As we move away from the isotropic point the boundary should be stretched in either the x or y direction.

To verify the metric (90) we compare the ratio between the height and width of the boundary w_y/w_x to the ratio of the principle axes of the ellipse d_x/d_y , given in (96). We find that at the isotropic point the width and height of the boundary are almost circular, with $w_y/w_x \approx 1$. Fig. 8 plots the comparison of w_y/w_x to d_x/d_y for different values of J_z . These ratios are in very close agreement with a deviation only near the phase transition points, $J_z = 0$ and $J_z = 2$, where the description we employed in Section II in terms of two Fermi points breaks down. We observe that an increase (decrease) in J_z corresponds

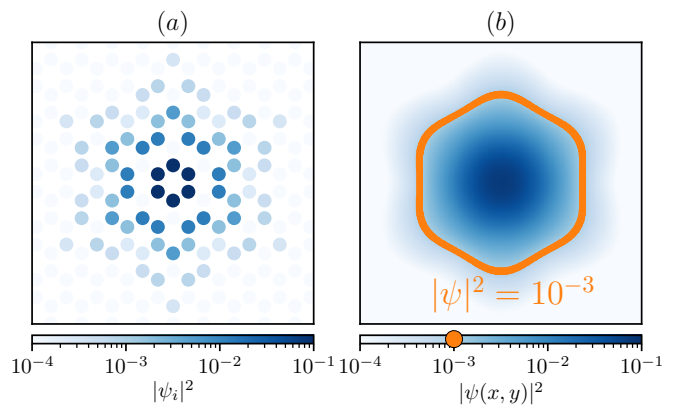


FIG. 9. Obtaining a continuous profile for the vortex and extracting its dimensions. (a) The lattice probability density $|\psi_i|^2$ of the wave function for a vortex, located on the plaquette in the centre. (b) A continuous approximation of the vortex probability distribution is constructed using two-dimensional Gaussians centred on each lattice site, as described in the text. The size and shape of the vortex are characterised by finding the set of points where $|\psi(\mathbf{r})|^2 = 10^{-3}$, as illustrated. Here we used $J_x = J_y = J_z = 1$, $K = 0.125$, $L = 36$ and $\epsilon = 1$.

to a decrease (increase) in the effective distance, d_y , resulting in stronger (weaker) correlations along that axis. Thus the correlations appear stretched (squeezed) along that axis of the lattice, i.e. an increase (decrease) in w_y/w_x .

B. Vortex zero-modes

Vortex excitations can be introduced by inserting π -fluxes into the \mathbb{Z}_2 gauge field that couples to the Majorana matter fermions of the model³³. Practically this can be done by flipping the sign of a coupling J_{ij} of a link (i, j) relative to its value in the no-vortex sector. This link belongs to two hexagonal plaquettes, and following this change of gauge, these two plaquettes will each hold a vortex. By subsequent changes in the sign of J_{ij} couplings these two vortices can be moved far apart. In the spectrum of the model the vortex pair manifests as a zero-energy fermion mode³³. By choosing a particular basis for this zero-energy fermion we can find fermionic creation operators that localise a fermion on only one of the vortices. In this way we can study the spatial wave function of a single vortex. Exactly diagonalising Hamiltonian (2) with a vortex pair inserted we find it is always possible to localise the wave function, provided the energy gap is large enough relative to the finite size discreteness of the spectrum. This gives a probability density at each lattice site, $|\psi_i|^2$, that we call the spatial profile of the wave function, as shown in Fig. 9(a).

To analyse the geometric profile of the zero modes we adopt the same procedure we used for the Majorana correlations. We approximate the lattice profile with a con-

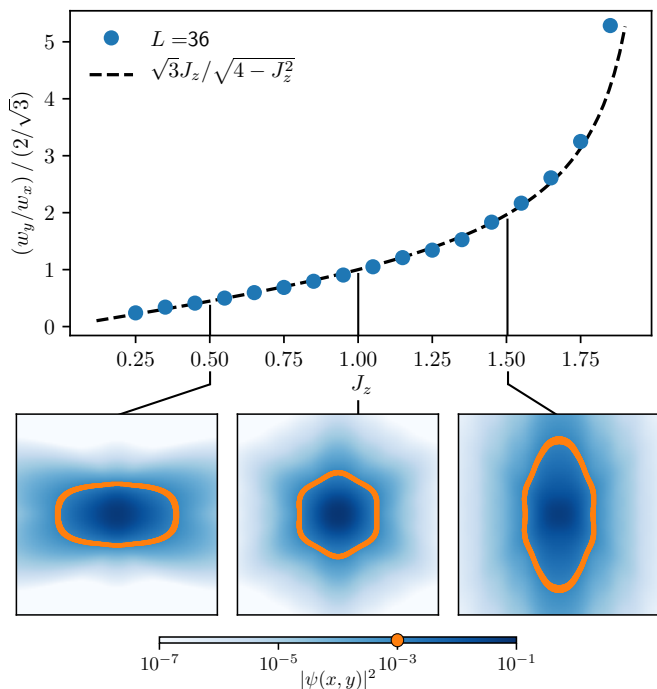


FIG. 10. Inferring the metric distortions from the spatial profile of a vortex wave function. The main panel plots the ratio between the height and width of the vortex boundary w_y/w_x , divided by the height to width ratio of a regular hexagon $2/\sqrt{3}$ for $J_x = J_y = 1$, $K = 0.125$, $\epsilon = 1$ and system size 36×36 . Also plotted with a dashed line is the theoretical relationship we expect from the geometrical description that is in very good agreement with the numerical data. Below are illustrative examples of the hexagonal boundaries we find. At the isotropic point, $J_z = 1$, it is a regular hexagon. As J_z deviates from the isotropic point the ratio w_y/w_x can take smaller or larger values than $2/\sqrt{3}$.

tinuous distribution by replacing each lattice point with two-dimensional Gaussians centred on each site,

$$|\psi(\mathbf{r})|^2 = \sum_i |\psi_i|^2 \delta(\mathbf{r} - \mathbf{r}_i) \rightarrow \sum_i \frac{|\psi_i|^2}{2\pi\epsilon} e^{-\frac{|\mathbf{r}-\mathbf{r}_i|^2}{2\epsilon}},$$

where ϵ is taken to be similar to the lattice spacing so that the Gaussians of neighbouring sites overlap. Fig. 9 illustrates this substitution. In the continuum we expect a single wave function exponentially localised at the position of the vortex. This continuous profile reduces the discrete lattice effects allowing us to clearly observe the effects of geometry.

From the continuous profile of the vortex we extract its relative scale in the x and y spatial directions by numerically identifying the set of points where $|\psi(\mathbf{r})|^2$ has decayed to a fixed value, e.g. 10^{-3} . This ‘boundary’ line is drawn for a vortex at the isotropic point of the model in Fig. 9(b). We observe that the geometry of the honeycomb lattice is strongly manifested in this boundary. This is due to the exponential localisation of the zero mode to the vortex, with localisation length comparable

to the lattice spacing and independent of the system size if we keep the energy gap constant. Hence, the lattice effects are expected to be visible in the wave function of the zero mode.

As we move away from the isotropic point the hexagon will be stretched in either the x or y direction. To compare the changing shape of the boundary to the distortions predicted by (96), we compare the ratio between the height and width of the hexagonal boundary w_y/w_x to the height and width ratio of a regular hexagon, $(2/\sqrt{3})$. We find that at the isotropic point the boundary satisfies $w_y/w_x = 2/\sqrt{3}$. Fig. 10 plots the comparison of $(w_y/w_x)/(2/\sqrt{3})$ to the ratio d_x/d_y , given in (96), for different values of J_z . We find that these ratios agree very well, particularly away from the phase transition boundaries. We observe that an increase (decrease) in J_z equates to a decrease (increase) in the effective distance, d_y . This results in the apparent stretching (squeezing) of the zero mode in that direction, i.e. an increase (decrease) in w_y/w_x . As a result the effective geometric description of KHLM in terms of a metric is faithful. As the metric is a geometric primitive, we expect that the rest of the geometric quantities, such as the curvature, to be faithfully reproduced as well. We leave this investigation to future work.

VI. CONCLUSIONS

In this paper we expanded upon the known result that the low energy limit, or continuum limit, of the Kitaev honeycomb lattice model is described by massless Majorana fermions obeying the Dirac Hamiltonian embedded in a flat Minkowski spacetime. We took this idea further by investigating whether the continuum limit could possibly yield non-trivial *curved* geometry. A suitable generalisation of Minkowski spacetime, namely a Riemann-Cartan geometry, with both curvature and torsion manifests itself in the KHLM via non-trivial dreibein e_a^μ and spacetime connection $\Gamma_{\mu\nu}^\rho = \tilde{\Gamma}_{\mu\nu}^\rho + K_{\mu\nu}^\rho$. It was shown that if the couplings of KHLM take a general space-dependent form, a Riemann-Cartan continuum limit can indeed be obtained.

We first showed theoretically that the single-particle Hamiltonian of a Majorana field in a Riemann-Cartan spacetime, h_{RC} , can be identified with the continuum limit of the KHLM Hamiltonian, h_{KHLM} , with general space-dependent nearest neighbour, $\{J_i\}$, and next-to-nearest neighbour, K , couplings. We demonstrated that the nearest-neighbour part of the Hamiltonian becomes the kinetic term of the Dirac-like continuum limit while the next-to-nearest neighbour part generates an energy gap at the Fermi points. By comparing h_{RC} and h_{KHLM} , we subsequently interpreted the coefficients of the kinetic term as the dreibein corresponding to a non-trivial Levi-Civita connection $\tilde{\Gamma}_{\mu\nu}^\rho$ and interpreted the K term that generates the gap as a non-trivial contortion $K_{\mu\nu}^\rho$. With this identification the metric $g_{\mu\nu} = e^a_\mu e^b_\nu \eta_{ab}$ was fully

determined, as well as the total connection $\Gamma^\rho_{\mu\nu} = \tilde{\Gamma}^\rho_{\mu\nu} + K^\rho_{\mu\nu}$, providing us with the curvature $R^\rho_{\mu\nu\sigma}$ and torsion $T^\rho_{\mu\nu}$ of the Riemann-Cartan theory.

For the special case of isotropic couplings where $J_x = J_y = J_z = J$, we demonstrated that the continuum limit had non-trivial dreibein and spacetime connection yielding a curvature and torsion depending on the parameters J and K . We also demonstrated that by modifying the model with a Kekulé distortion, one can give the Majorana fermions a non-zero mass in the continuum limit. To study the anisotropic case we considered in detail the special configuration of couplings where $J_x = J_y = 1$, with J_z a free parameter. In this case, the metric of the continuum limit corresponded to a non-uniform dilation in the x - and y -directions relative to the isotropic metric. This stretching of space was confirmed by analysing the spatial distribution of the quantum correlations as well as the zero-mode profiles of the model. We numerically determined that the description of the model in terms of a geometric metric is faithful even for moderate system sizes. In Fig. 8 and Fig. 10 we see how well the geometric theory describes the deformation of the quantum correlations and zero mode profiles, respectively.

Our work verified that the theory of Majorana fields in Riemann-Cartan geometry can faithfully describe the microscopic Kitaev honeycomb lattice model. This field

theoretic description can be then employed to analytically investigate a variety of properties of the microscopic model. For example, this opens up the exciting possibility to quantitatively study the energy-momentum currents of KHLM and determine their behaviour in terms of various coupling configurations or external driving. Moreover, chiral gauge fields have been investigated in the context of graphene⁶² that could be extended to the KHLM case, giving a more complete quantum field theory description of the model. Finally, the response of KHLM to time-dependent geometric perturbations including quenches⁶³ can also be probed using the formalism developed here. We leave these investigations to a future work.

ACKNOWLEDGMENTS

We would like to thank Duncan Haldane, Paolo Maraner, Jaakko Nissinen, Joost Slingerland and Christopher J. Turner for inspiring conversations. This work was supported by the EPSRC grant EP/R020612/1. Statement of compliance with EPSRC policy framework on research data: This publication is theoretical work that does not require supporting research data.

[†] A.F. and M.D.H. contributed equally to this work

¹ X. G. Wen and A. Zee, *Phys. Rev. Lett.* **69**, 953 (1992).
² J. E. Avron, R. Seiler, and P. G. Zograf, *Phys. Rev. Lett.* **75**, 697 (1995).
³ N. Read, *Phys. Rev. B* **79**, 045308 (2009).
⁴ F. D. M. Haldane, ArXiv e-prints (2009), arXiv:0906.1854 [cond-mat.str-el].
⁵ A. G. Abanov and A. Gromov, *Phys. Rev. B* **90**, 014435 (2014).
⁶ A. Gromov, G. Y. Cho, Y. You, A. G. Abanov, and E. Fradkin, *Phys. Rev. Lett.* **114**, 016805 (2015).
⁷ B. Bradlyn and N. Read, *Phys. Rev. B* **91**, 125303 (2015).
⁸ T. Can, M. Laskin, and P. Wiegmann, *Phys. Rev. Lett.* **113**, 046803 (2014).
⁹ S. Klevtsov and P. Wiegmann, *Phys. Rev. Lett.* **115**, 086801 (2015).
¹⁰ T. L. Hughes, R. G. Leigh, and E. Fradkin, *Phys. Rev. Lett.* **107**, 075502 (2011).
¹¹ A. Gromov and A. G. Abanov, *Phys. Rev. Lett.* **113**, 266802 (2014).
¹² S. M. Girvin, A. H. MacDonald, and P. M. Platzman, *Phys. Rev. Lett.* **54**, 581 (1985).
¹³ F. D. M. Haldane, *Phys. Rev. Lett.* **107**, 116801 (2011).
¹⁴ A. Gromov and D. T. Son, *Phys. Rev. X* **7**, 041032 (2017).
¹⁵ P. Wiegmann, *Phys. Rev. Lett.* **120**, 086601 (2018).
¹⁶ O. Golan and A. Stern, *Phys. Rev. B* **98**, 064503 (2018).
¹⁷ F. Hehl and B. Datta, *Journal of Mathematical Physics* **12**, 1334 (1971).
¹⁸ M. Katanaev and I. Volovich, *Annals of Physics* **216**, 1 (1992).

¹⁹ F. de Juan, A. Cortijo, and M. Vozmediano, *Nucl. Phys. B* **828**, 625 (2010).
²⁰ G. Palumbo and J. K. Pachos, *Annals of Physics* **372**, 175 (2016).
²¹ P. Maraner, J. K. Pachos, and G. Palumbo, *Scientific Reports* **9**, 17308 (2019).
²² J. Nissinen, (2019), arXiv:1909.05846.
²³ J. M. Luttinger, *Phys. Rev.* **135**, A1505 (1964).
²⁴ R. Nakai, S. Ryu, and K. Nomura, *New Journal of Physics* **18**, 023038 (2016).
²⁵ N. R. Cooper, B. I. Halperin, and I. M. Ruzin, *Phys. Rev. B* **55**, 2344 (1997).
²⁶ N. Read and D. Green, *Phys. Rev. B* **61**, 10267 (2000).
²⁷ Z. Wang, X.-L. Qi, and S.-C. Zhang, *Phys. Rev. B* **84**, 014527 (2011).
²⁸ S. Ryu, J. E. Moore, and A. W. W. Ludwig, *Phys. Rev. B* **85**, 045104 (2012).
²⁹ T. Qin, Q. Niu, and J. Shi, *Phys. Rev. Lett.* **107**, 236601 (2011).
³⁰ A. Shitade, *Progress of Theoretical and Experimental Physics* **2014**, 123I01 (2014).
³¹ S. Jezouin, F. D. Parmentier, A. Anthore, U. Gennser, A. Cavanna, Y. Jin, and F. Pierre, *Science* **342**, 601 (2013).
³² M. Banerjee, M. Heiblum, A. Rosenblatt, Y. Oreg, D. E. Feldman, A. Stern, and V. Umansky, *Nature* **545**, 75 (2017).
³³ A. Kitaev, *Annals of Physics* **321**, 2 (2006), january Special Issue.
³⁴ A. Kitaev, *Annals of Physics* **303**, 2 (2003).

- ³⁵ D. Otten, A. Roy, and F. Hassler, *Phys. Rev. B* **99**, 035137 (2019).
- ³⁶ G. Moore and N. Read, *Nuclear Physics B* **360**, 362 (1991).
- ³⁷ V. Lahtinen, G. Kells, A. Carollo, T. Stitt, J. Vala, and J. K. Pachos, *Annals of Physics* **323**, 2286 (2008).
- ³⁸ C. N. Self, J. K. Pachos, J. R. Wootton, and S. Iblisdir, *Phys. Rev. B* **95**, 115141 (2017).
- ³⁹ C. N. Self, J. Knolle, S. Iblisdir, and J. K. Pachos, *Phys. Rev. B* **99**, 045142 (2019).
- ⁴⁰ V. Lahtinen and J. K. Pachos, *Phys. Rev. B* **81**, 245132 (2010).
- ⁴¹ V. Lahtinen, A. W. W. Ludwig, J. K. Pachos, and S. Trebst, *Phys. Rev. B* **86**, 075115 (2012).
- ⁴² J. Nasu, M. Udagawa, and Y. Motome, *Phys. Rev. Lett.* **113**, 197205 (2014).
- ⁴³ J. Nasu, M. Udagawa, and Y. Motome, *Phys. Rev. B* **92**, 115122 (2015).
- ⁴⁴ J. Nasu and Y. Motome, *Phys. Rev. Lett.* **115**, 087203 (2015).
- ⁴⁵ J. c. v. Chaloupka, G. Jackeli, and G. Khaliullin, *Phys. Rev. Lett.* **105**, 027204 (2010).
- ⁴⁶ S. K. Choi, R. Coldea, A. N. Kolmogorov, T. Lancaster, I. I. Mazin, S. J. Blundell, P. G. Radaelli, Y. Singh, P. Gegenwart, K. R. Choi, S.-W. Cheong, P. J. Baker, C. Stock, and J. Taylor, *Phys. Rev. Lett.* **108**, 127204 (2012).
- ⁴⁷ G. Jackeli and G. Khaliullin, *Phys. Rev. Lett.* **102**, 017205 (2009).
- ⁴⁸ A. Banerjee, C. Bridges, J.-Q. Yan, A. Aczel, L. Li, B. Stone, G. Granroth, M. Lumsden, Y. Yiu, J. Knolle, S. Bhattacharjee, D. Kovrizhin, R. Moessner, D. Tennant, D. Mandrus, and S. Nagler, *Nature Materials* **15**, 733 (2016).
- ⁴⁹ Z.-C. Yang, T. Iadecola, C. Chamon, and C. Mudry, *Phys. Rev. B* **99**, 155138 (2019).
- ⁵⁰ A. H. Castro Neto, F. Guinea, N. M. R. Peres, K. S. Novoselov, and A. K. Geim, *Rev. Mod. Phys.* **81**, 109 (2009).
- ⁵¹ D. P. DiVincenzo and E. J. Mele, *Phys. Rev. B* **29**, 1685 (1984).
- ⁵² G. W. Semenoff, *Phys. Rev. Lett.* **53**, 2449 (1984).
- ⁵³ L. Savary and L. Balents, *Reports on Progress in Physics* **80**, 016502 (2017).
- ⁵⁴ L. Balents, *Nature* **464**, 199 (2010).
- ⁵⁵ J. Knolle and R. Moessner, *Annual Review of Condensed Matter Physics* **10**, 451 (2019).
- ⁵⁶ M. Nakahara, *Geometry, Topology and Physics*, 2nd ed. (Taylor & Francis Group, 2003).
- ⁵⁷ S. Carroll, *Spacetime and Geometry: An Introduction to General Relativity*, 1st ed. (Pearson, 2003).
- ⁵⁸ C.-Y. Hou, C. Chamon, and C. Mudry, *Phys. Rev. Lett.* **98**, 186809 (2007).
- ⁵⁹ C.-K. Chiu, J. C. Y. Teo, A. P. Schnyder, and S. Ryu, *Rev. Mod. Phys.* **88**, 035005 (2016).
- ⁶⁰ R. Jackiw and P. Rossi, *Nuclear Physics B* **190**, 681 (1981).
- ⁶¹ K. Meichanetzidis, C. J. Turner, A. Farjami, Z. Papić, and J. K. Pachos, *Phys. Rev. B* **97**, 125104 (2018).
- ⁶² R. Jackiw and S.-Y. Pi, *Phys. Rev. Lett.* **98**, 266402 (2007).
- ⁶³ Z. Liu, A. Gromov, and Z. Papić, *Phys. Rev. B* **98**, 155140 (2018).

Appendix A: Hermiticity of the Dirac Hamiltonian in curved spacetime

It is worth commenting on the Hermiticity of the Hamiltonian (45). When discussing the Hermiticity of an operator we must have an inner product in mind. We define the Hermitian conjugate, or adjoint, of an operator O on some vector space V as the operator O^\dagger defined by $\langle \psi | O \phi \rangle = \langle O^\dagger \psi | \phi \rangle$ for all $\psi, \phi \in V$, where $\langle \cdot | \cdot \rangle$ is the inner product on V . The natural inner product between single-particle spinor wavefunctions ψ and ϕ defined on a curved spacetime M is given by

$$\langle \psi | \phi \rangle = \int_M d^{2+1}x |e| \bar{\psi}(x) \phi(x). \quad (\text{A1})$$

We know from quantum mechanics on a flat spacetime that the four-momentum operator $p_\mu = -i\partial_\mu$ is an Hermitian operator, however in curved space it is no longer Hermitian:

$$\begin{aligned} \langle \psi | p_\mu \phi \rangle &= \int_M d^{2+1}x |e| \bar{\psi}(-i\partial_\mu \phi) \\ &= \int_M d^{2+1}x [-i\partial_\mu(|e|\bar{\psi}\phi) + i(\partial_\mu|e|)\bar{\psi}\phi + i|e|(\partial_\mu\bar{\psi})\phi] \\ &= \int_M d^{2+1}x [|e| i\tilde{\omega}_{\mu a}^a \bar{\psi}\phi + |e| \overline{(-i\partial_\mu\psi)} \phi] \\ &= \langle p_\mu \psi | \phi \rangle + \langle \psi | i\tilde{\omega}_{\mu a}^a \phi \rangle \end{aligned} \quad (\text{A2})$$

where we have integrated by parts and ignored the boundary term. The solution to this conundrum is to redefine our momentum operator as

$$p_\mu = -i \left(\partial_\mu + \frac{1}{2} \tilde{\omega}_{\mu a}^a \right) \quad (\text{A3})$$

and we find that Hermiticity is indeed restored as $\langle \psi | p_\mu \phi \rangle = \langle p_\mu \psi | \phi \rangle$.

To check that this is a valid momentum operator, we must ensure that it obeys the canonical commutator $[x^\mu, p_\nu] = i\delta_\nu^\mu$. We can see this explicitly by considering an arbitrary test spinor ψ :

$$\begin{aligned} [x^\mu, p_\nu] \psi &= -ix^\mu \left(\partial_\nu + \frac{1}{2} \tilde{\omega}_{\nu a}^a \right) \psi + i \left(\partial_\nu + \frac{1}{2} \tilde{\omega}_{\nu a}^a \right) x^\mu \psi \\ &= -ix^\mu \partial_\nu \psi - \frac{i}{2} x^\mu \tilde{\omega}_{\nu a}^a \psi + i\partial_\nu(x^\mu \psi) + \frac{i}{2} \tilde{\omega}_{\nu a}^a x^\mu \psi \\ &= i\delta_\nu^\mu \psi. \end{aligned} \quad (\text{A4})$$

Therefore the operator is indeed a valid momentum operator.

From these results we can see that the Hamiltonian (45) is Hermitian because $\langle \psi | h \phi \rangle = \langle h \psi | \phi \rangle$ for all spinors ψ and ϕ .